Full Length Article

# Measurement of anisotropic thermal conductivity and inter-layer thermal contact resistance in polymer fused deposition modeling (FDM)

Hardikkumar Prajapati, Darshan Ravoori, Robert L. Woods, Ankur Jain*

*Mechanical and Aerospace Engineering Department, University of Texas at Arlington, Arlington, TX, USA*

## ARTICLE INFO

## ABSTRACT

Additive manufacturing, or 3D printing, is an exciting manufacturing technique based on layer-by-layer build-up as opposed to the subtractive approach in most traditional machining processes. Specifically, in polymer-based additive manufacturing processes, filaments of a polymer are dispensed from a rastering extruder to define each layer. Due to the directional nature of this process, it is of interest to determine whether thermal transport properties of the built part are direction dependent. Such an understanding is critical for accurate design of components that serve a thermal function. This paper reports measurement of thermal conductivity of additively manufactured polymer samples in the filament rastering direction and in the build direction. Samples are designed and built in order to force heat flow only in one direction during thermal property measurement. Experimental data indicate significant anisotropy in thermal conductivity, with the value in the build direction being much lower than in the raster direction. Both thermal conductivities are found to depend strongly on the air gap between adjacent filaments. A theoretical thermal conduction model is found to be in good agreement with experimental data. These measurements are also used to determine the inter-layer thermal contact resistance, which is found to be a non-monotonic function of the air gap. Cross section images of samples confirm the strong effect of the gap on the microstructure, and hence on thermal properties. Results from this paper provide a key insight into the anisotropic nature of thermal conduction in additively manufactured components, and establish the presence of significant inter-layer thermal contact resistance. These results may be helpful in the fundamental understanding of heat transfer in 3D-printed components, as well as in accurate design and fabrication of heat transfer components through 3D printing.

## 1. Introduction

Additive manufacturing techniques [1–3] are being widely investigated for a large number of engineering [1,4,5] and biomedical applications [6–9]. These techniques rely on layer-by-layer part fabrication instead of the top-down, subtractive approach in most traditional machining technologies [2,3,10]. Several additive manufacturing techniques are based on an energy source that rasters over a powder bed and causes selective melting and solidification to form the desired shape [2,3,10–12]. In other techniques, a rastering extruder dispenses material, usually a polymer on to a bed at a temperature greater than its glass transition temperature [2,3,10]. In each case, the part is built layer by layer, therefore offering close control of the part building process and dramatically expanding the design space available for the built part. For example, the ability of additive manufacturing to build parts of almost arbitrary shape and cross-section significantly increases the choice of feasible shapes and sizes for many parts. However, because these techniques are additive in nature and do not start with a

fully dense, solid part, additive manufacturing also introduces several challenges related to functional properties such as strength, thermal conductivity, etc. of the eventual part [13].

While several additive manufacturing techniques have been used for rapid prototyping of model parts for a long time [3], there has been much recent focus on the use of these techniques for building functional parts capable of withstanding thermal/mechanical loads such as stresses, heat fluxes, etc. [1]. Fused Deposition Modeling (FDM) [14] is a commonly used additive manufacturing process, in which an extruder rasters across a bed and dispenses filaments of a polymer above its glass transition temperature. By selectively dispensing the polymer, nearly any cross-section can be built. Once a layer has been built, the extruder rasters and dispenses again in order to build the next layer. Since the porosity of parts can be well controlled in the FDM process by changing the air gap between adjacent raster lines, it can be used for building parts for thermal insulation applications that call for low weight and low thermal conductivity. However, given the complex nature of additive manufacturing techniques, it is critical to examine the

---
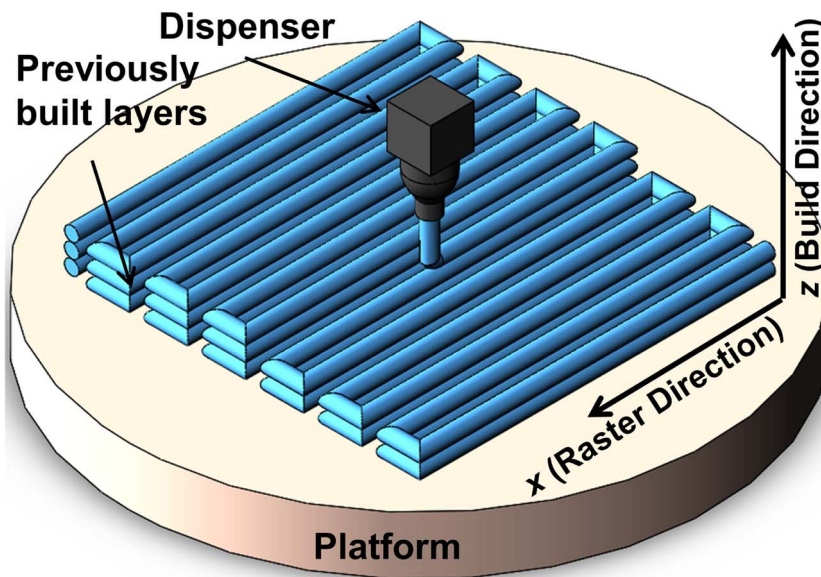
**Fig. 1.** General schematic of the filament rastering process in Fused Deposition Modeling (FDM) for polymer-based additive manufacturing.

fundamental transport processes in FDM, and understand the dependence of functional properties of built parts on process parameters. Such an understanding will help optimize additive manufacturing process to build parts of desired properties and function.

Fig. 1 shows a general schematic of the material deposition process during a FDM process. The raster direction, in which the extruder moves during the dispensing process is taken to be along the $x$ axis. Once one layer has been fully built, the extruder dispenses the next layer, so that the part grows in the build direction, taken to be the $z$ axis. Due to the directional nature of deposition in FDM, it is likely that properties of the built part may be direction-dependent. Several papers have reported anisotropic mechanical properties of FDM-built parts [15–20]. In most cases, the part is found to have the highest strength in the direction in which the material is deposited ($x$ direction as shown in Fig. 1). This is likely due to better material continuity and fewer material interfaces along the $x$ direction compared to the $z$ direction in which interfaces between successive layers may result in reduced strength.

Due to the unique nature of FDM process, thermal conductivity of the built part is likely to deviate from thermal conductivity of the pristine material. Direct measurement of thermal properties of the FDM built part is therefore critical. Further, due to the unique distinction between raster and build directions, thermal conductivity is also expected to be different in the two directions. While there is a reasonable amount of literature on anisotropic mechanical properties of FDM-built parts [15–18], there is very little available literature on the investigation of thermal transport properties such as thermal conductivity of FDM-built parts. For example, Weng, et al. report thermal expansion coefficient of FDM-built ABS parts, but do not report thermal conductivity [21]. Other papers that measure thermal conductivity often only report a single value of this property, and do not account for possible variations in different directions [22]. Shemelya, et al. have used the transient plane source method to measure the in-plane and out-of-plane thermal conductivities of FDM-built parts [23]. Some dependence on the filament material has been reported, although the effect of process and design parameters such as raster width and air gap has not been studied. Chung, et al. [24] have also presented similar measurements to understand the effect of random voids. However, due to the randomness of voids introduced into this work, it is difficult to make any conclusions about the inherent dependence of these properties on process parameters. In addition to anisotropic thermal conductivity, the thermal contact resistance that may exist between

successive layers in the $z$ direction due to the presence of interfaces has also not been reported. Such interfacial thermal resistance may impede the flow of heat in $z$ direction in a similar manner as the impact on mechanical strength [16,18], and reduce the $z$-direction thermal conductivity compared to the $x$ direction. The lack of such data may partly be due to the significant difficulties in experimental measurement of direction-dependent thermal properties. Such a measurement requires samples with consistently aligned raster lines. This is often not available as part of standard processes on commercial FDM tools which by default produce parts with hatched line configurations. Further, forcing heat flow in a single direction during a thermal property measurement and embedding temperature sensors in successive layers in order to measure the interfacial temperature difference are also not straightforward. Despite these difficulties, characterization of anisotropic thermal transport in FDM parts is very important for understanding the fundamental relationships between process parameters and thermal properties of the built part. Such an understanding will help design FDM process flows for building parts with exceptional thermal functionality, such a ultra-low thermal conductivity, or highly directional thermal transport. A good understanding of thermal contact resistance between successive layers could potentially be used to tailor thermal properties without affecting other performance parameters. This could contribute towards understanding and reconciling multiphysics design trade-offs that exist between thermal performance, mechanical performance and weight of the built part.

This paper presents experimental measurement of anisotropic thermal conductivity and inter-layer thermal contact resistance in FDM-built parts. Measurements indicate that there exists strong anisotropy in thermal conduction in these parts, wherein thermal conductivity in the $z$ direction is significantly lower than in the $x$ direction. These thermal conductivity values are found to be functions of the air gap between filament lines during the deposition process. Experimental measurements are found to be in good agreement with an analytical model of thermal conduction developed in this paper. Further, a significant thermal contact resistance between successive layers is measured, and found to be a non-monotonic function of the air gap. These measurements provide a previously-unavailable insight into the fundamental nature of thermal conduction in parts built by additive manufacturing. The anisotropy in thermal conduction, as well as thermal contact resistance measured here could potentially be used for designing and building parts with novel thermal functionality, such as parts with ultra-low thermal conductivity and/or highly directional heat flow.

## 2. Experiments

### 2.1. Sample preparation

All tested sample are fabricated on Stratasys Fortus 450 mc with ABS and ULTEM thermoplastic materials. Solid models of samples are prepared using a CAD software and converted into .stl files. These digital models are then sliced using Insight software, and tool paths of extruder are exported in .cmb format. In these experiments, the height of each layer is 0.25 mm, and raster width is 0.41 mm with multiple values of the air gap (eight for ABS and seven for ULTEM). The air gaps are chosen to be 0 mm, 0.127 mm, 0.203 mm, 0.254 mm, 0.3810 mm, 0.6350 mm and 0.7620 mm for both materials. An additional air gap of 0.508 mm is chosen for ABS. Two sets of such samples are built, such that either the build or direction is oriented with the thickness of the sample. All the raster lines in each layer are stacked in the same orientation. This deviates from the default practice of dispensing filaments at ± 45° orientation in alternating layers. This is done to force heat flow in only one direction – raster or build – and therefore measure the directional thermal conductivity. Default values are chosen for all other settings such as extruder speed, dispense temperature for the main and supporting material, etc. Samples of 25.4 mm by 25.4 mm size and two different thicknesses – 5 mm and 8 mm – are built in order to facilitate thermal conductivity measurement using the 1D steady state heat flux method [25].

### 2.2. Thermal conductivity measurement

The primary thermal property of interest for additively manufactured samples is the thermal conductivity in raster and build directions, which can be determined from the amount of heat flux in a particular direction for a given temperature gradient in that direction. The directional thermal conductivity of additively manufactured samples is measured by a heat flow meter instrument (FOX50, LaserComp-TA Instruments), as shown in Fig. 2. This instrument utilizes the two thickness method. In this method, a sample is sandwiched between two flat isothermal plates maintained at different temperatures. One-dimensional heat transfer occurs through the sample, eventually resulting in a steady-state one-dimensional temperature field within the sample. Temperatures of the two plates are measured through embedded thermocouples. An insulating guard is provided around the sample to minimize stray heat loss. Heat flux is measured in both plates to confirm that there is minimal stray heat loss. Based on Fourier's law, the total thermal resistance of the sample of thickness $L_1$, which comprises material resistance through the sample, and the two thermal resistances between sample surface and instrument, can be determined from

$$R_1 = \frac{L_1}{k} + 2R_{\{s-i\}} = \frac{\Delta T}{Q_1} \tag{1}$$

where $Q_1$ is the measured heat flux resulting from the imposed temperature gradient and $R_{\{s-i\}}$ refers to the thermal contact resistance between sample and instrument. If the same measurement is repeated with a sample of thickness $L_2$ at the same temperature gradient, resulting in a measured heat flux of $Q_2$, then the thermal conductivity of the material being tested can be determined from

$$k = \frac{Q_1 Q_2 (L_1 - L_2)}{(Q_2 - Q_1)\Delta T} \tag{2}$$

where the sample-to-instrument thermal contact resistance is assumed to remain the same in both experiments.

In these experiments, the sample thicknesses are chosen to be 8 mm and 5 mm in order to stay within the instrument's heat flux measurement capability. Further, each measurement is carried out twice to ensure repeatability.

### 2.3. Visualization of cross section of samples

After thermal property measurements, samples are cut in the *yz* plane in order to visualize the internal structure of the samples. Since ABS and ULTEM are thermoplastic, the use of conventional cutting tools is found to be ineffective, as it leads to removal and re-deposition of material on the internal structure during the cutting process. Instead, a small, the lead cut is made in the sample, which is then soaked in liquid nitrogen for 2–3 mins [26]. This makes the sample temporarily brittle, which can be easily broken by applying an impact load on the lead cut. This results in preservation of the internal structure of the sample, making it possible to accurately image the cross-section. A Nikon Eclipse ME600 microscope is used for visualization.

## 3. Theoretical modeling of thermal conductivity and thermal contact resistance

Test samples printed using the procedure outlined in Section 2 comprise aligned filaments certain width and a certain air gap between adjacent filaments. In these experiments, each layer is built with the same filament orientation. In order to consolidate the part, the outer surfaces of the part are usually printed with zero air gap. Since this covers only a small fraction of the part along the outside edges, estimated to be less than 5%, it is reasonable to neglect this for heat transfer analysis, and assume heat transfer in the part to be driven by thermal resistances through the filament material and air gap, and by inter-layer thermal contact resistances. While the final shape of the filament may be quite complicated, as an approximation, each filament is assumed to be a parallelepiped, with a width $w_f$ in the cross section, shown schematically in Fig. 3(b) . The air gap between adjacent filaments is assumed to be $w_a$. Assuming that the total number of layers is $n$, heat transfer in the raster direction (*x* axis as shown in Fig. 1) comprises $n$ thermal resistances in parallel, each of which represent the thermal resistance of a layer. The thermal resistance of each layer in turn comprises *x*-direction thermal resistances from the filament and air gap, arranged in parallel. Assuming the thermal conductivities of the filament and air to be $k_f$ and $k_a$ respectively, the effective thermal conductivity of the additively manufactured part in the raster direction is found through the series-parallel combinations of thermal resistances to be
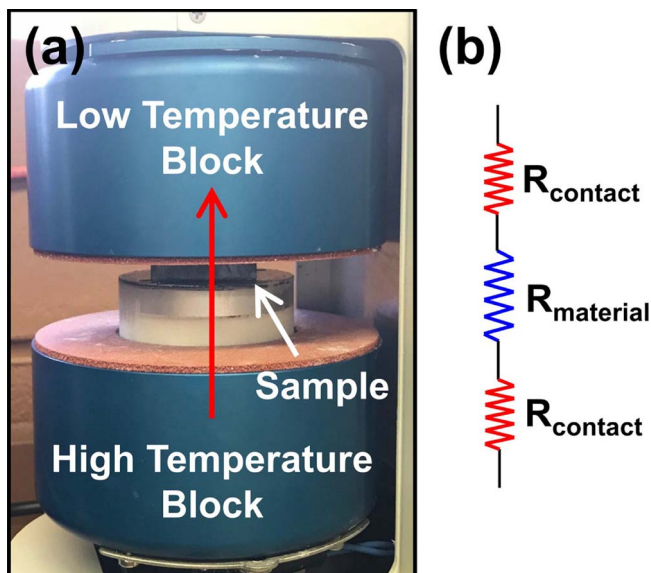


**Fig. 2.** (a) Picture of the experimental setup based on one-dimensional steady state heat flux for measurement of thermal conductivity of additively manufactured components; (b) Schematic of the key thermal resistances involved in this measurement.
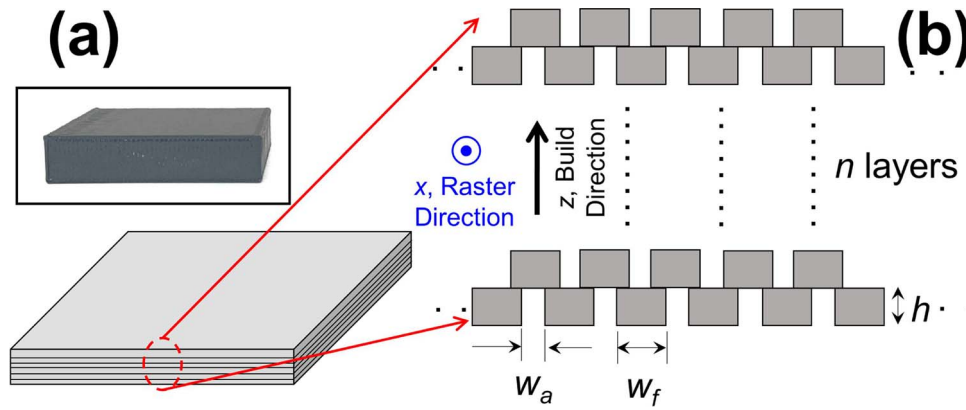
**Fig. 3.** (a) Overall schematic of a FDM-printed part, also showing a picture of a sample printed in this work; (b) Schematic model of the internal geometry of an additively manufactured component showing the filament and air components in the thermal resistance network in a single layer, and in the entire part comprising multiple layers in the build direction.

$$k_x = \frac{w_a k_a + w_f k_f}{w_a + w_f} \tag{3}$$

In the build direction ($z$ direction as shown in Fig. 1), the thermal resistances of the $n$ layers are arranged in series. Thermal resistance of each layer in turn comprises $z$-direction thermal resistances of the filament and air gap arranged in parallel. In addition, interfacial thermal contact resistance between adjacent layers also contributes towards total thermal resistance in the build direction. Combining all these contributions, the effective thermal conductivity in the build direction is found to be

$$\frac{1}{k_z} = \frac{w_a + w_f}{w_a k_a + w_f k_f} + \frac{R_c}{h} \tag{4}$$

where $R_c$ is the thermal contact resistance between adjacent layers and $h$ is the layer height.

Note from Eqs. (3) and (4), that in the absence of $R_c$, $k_x$ and $k_z$ are equal to each other. However, due to the presence of non-zero thermal contact resistance occurring due to imperfect thermal contact between adjacent layers, Eqs. (3) and (4) show that $k_z$ will be lower than $k_x$, thereby resulting in thermal conduction anisotropy in the additively manufactured part.

Eqs. (3) and (4) show that $R_c$ can be determined from measured values of $k_x$ and $k_z$ as follows:

$$R_c = h\left(\frac{1}{k_z} - \frac{1}{k_x}\right) \tag{5}$$

Eqs. (3) and (4) also show that both $k_x$ and $k_z$ are functions of process and design parameters, including filament material, raster width and air gap. This indicates the possibility of tuning effective thermal conductivities in both directions by changing these process and design parameters.

The next section presents results from experimental measurements of thermal conductivities in the raster and build directions, as well as the interfacial thermal contact resistance obtained from Eq. (5). Comparison of experimental data with analytical model results is also discussed.

## 4. Results and discussion

Thermal conductivity in the raster direction ($x$ axis, as shown in Fig. 1) is measured for two different filament materials, ABS and ULTEM for a number of values of $w_a$, the air gap between filament lines. For these experiments, the filament line width, $w_f$, is held constant at 0.41 mm. Samples of thicknesses 5 mm and 8 mm, in which the raster direction coincides with the axial direction of the thermal conductivity measurement setup shown in Fig. 2 are designed and built. Fig. 4(a) and (b) plot the measured thermal conductivity in raster direction, $k_x$ as a

function of air gap, $w_a$ for ABS and ULTEM respectively. The theoretical relationship between the two based on Eq. (3) from Section 3 is also plotted in these figures. Fig. 4 shows that as the air gap increases, thermal conductivity in the raster direction reduces significantly for both materials in a similar fashion. This occurs primarily because of the increased fraction of air gap in the cross-section, and therefore increased resistance to heat flow in the $x$ direction. Experimental data are in good agreement with the curve representing the analytical model, which shows that the nature of heat transfer in the raster direction is well described by an appropriate series/parallel combination of thermal resistances through the material and air gaps. Even though the analytical modeling is carried out assuming rectangular cross-section of the extruded filaments, it nevertheless results in good agreement with experimental data. As the air gap increases from 0 mm to 0.76 mm in the case of ABS, there is a 54% reduction in $k_x$, which may be quite significant. There is some departure between thermal conductivity measurements and theoretical model when the air gap is very large. This is believed to occur because at large air gaps, filaments are not well supported by filaments in the underlying layer, due to which some mechanical distortion of the filaments might occur and cause minor departure from the microstructure assumed by the theoretical model.

The relationship between design parameters such as $w_a$ and ultimate thermal properties of the part as shown in Fig. 4 is corroborated by cross-section imaging of these samples. Fig. 5 shows cross-sections of ABS samples with zero and 0.25 mm air gap, at a filament width of 0.41 mm. These images clearly show change in the microstructure as the air gap increases, which causes the reduction in the measured raster-direction thermal conductivity. Fig. 5 shows some distortion in the cross section of the filaments, particularly at low air gaps. However, because of the higher thermal resistance through the air gap compared to the filament, this is not expected to dramatically impact overall thermal conductivity.

Experiments are then carried out to measure thermal conductivity in the build direction, $k_z$ for multiple values of air gap while the filament width is fixed at 0.41 mm, similar to measurements of thermal conductivity in the raster direction. Similar to previous experiment, samples of 5 mm and 8 mm thicknesses in which the build direction is aligned with the axial direction of the thermal conductivity measurement setup are designed and fabricated. Fig. 6 plots these data and shows, similar to Fig. 4, a reduction in $k_z$ as the air gap increases. Measurements indicate that at any value of the air gap, thermal conductivity in the build direction, $k_z$, is significantly lower than in the raster direction, $k_x$. This establishes that thermal conductivity in the FDM-built part is significantly anisotropic. The built part offers greater impedance to heat flow in the build direction, $z$, than in the raster direction, $x$. This anisotropy, which may be represented by the ratio $k_z/k_x$ is also plotted in Fig. 6. Fig. 6 shows that the degree of anisotropy starts at close to 1.0 when the air gap is zero, and reduces sharply as the air
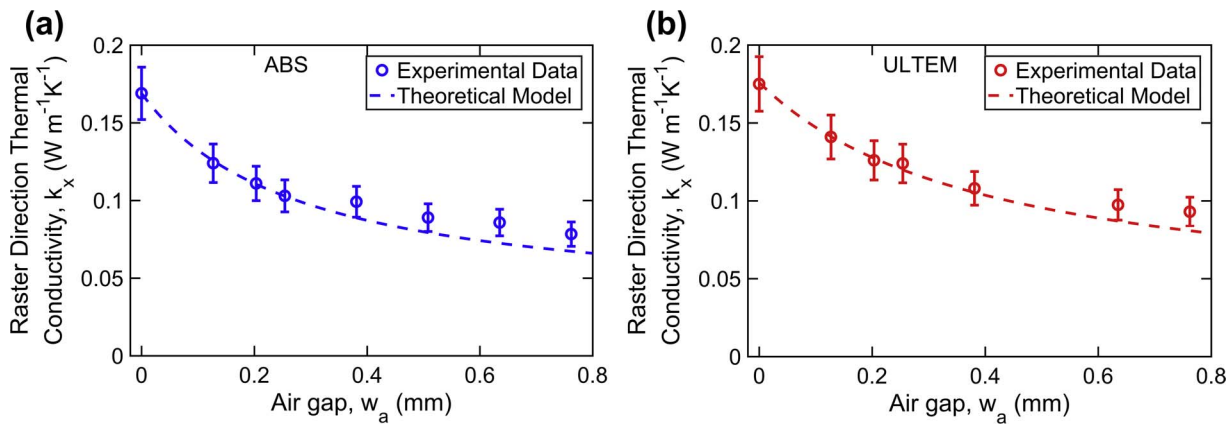
**Fig. 4.** Measured thermal conductivity in the raster direction, $k_x$, as a function of air gap for (a) ABS; and (b) ULTEM filament materials. Predicted curves from the analytical model, Eq. (3) are also plotted in each case.
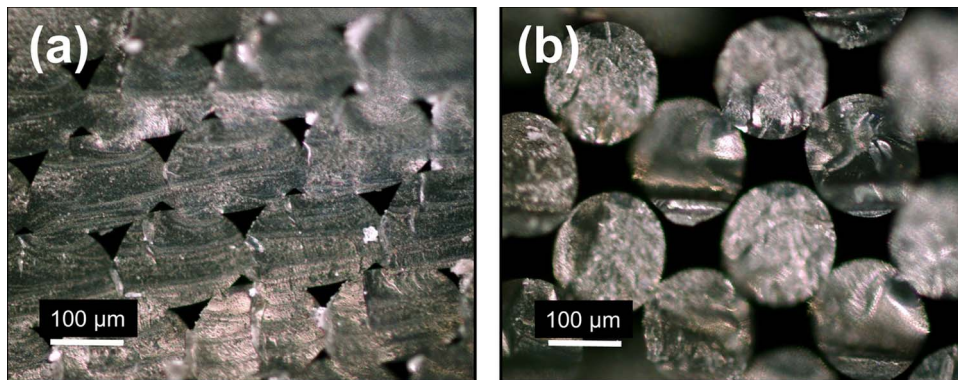


**Fig. 5.** Cross section images of two ABS samples with (a) zero; and (b) 0.25 mm air gap, showing significant difference in microstructure. In each case, the raster direction, *x*, is normal to the plane of the image.
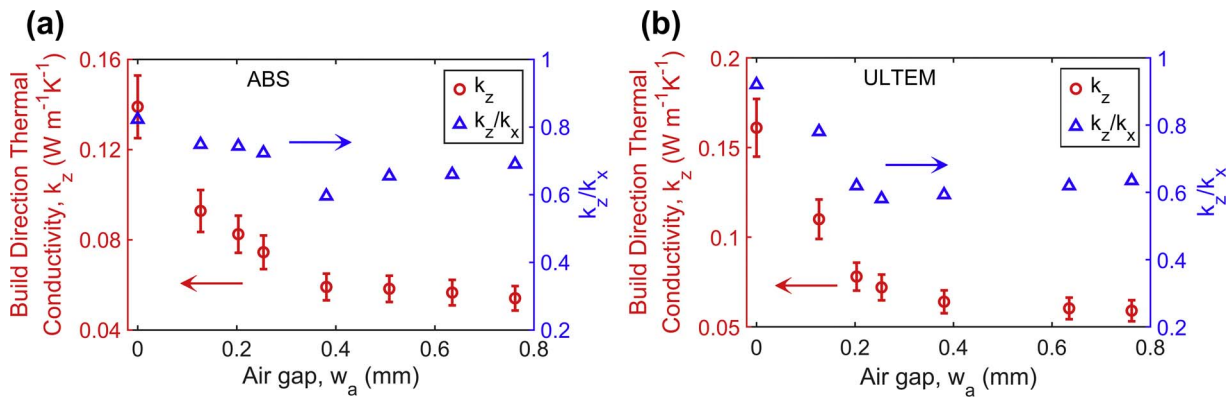


**Fig. 6.** Measured thermal conductivity in the build direction, $k_z$, as a function of air gap for (a) ABS; and (b) ULTEM filament materials. The ratio $k_z/k_x$, which represents the degree of anisotropy is also plotted in each case.

gap increases. Eventually, this ratio plateaus out at large values of the air gap. The ratio $k_z/k_x$ is found to be as low as 0.60 at large air gap, which represents significant anisotropy in thermal conduction.

The observation that thermal conductivity in the build direction, $k_z$ is always lower than in the raster direction, $k_x$ establishes the presence of significant thermal contact resistance at the interfaces between successive layers in the part. Data shown in Figs. 4 and 5 are consistent with the theoretical model presented in section 3, specifically Eqs. (3) and (4), which predict lower thermal conductivity in the build direction than in the raster direction. due to the presence of thermal contact resistance at interfaces between successive layers. The value of the interfacial thermal contact resistance at any specific air gap can be determined by using measured values of $k_x$ and $k_z$ in Eq. (5). Thermal

contact resistance computed in this manner is plotted as a function of air gap in Fig. 7, which shows that as the air gap increases, thermal contact resistance also goes up. This shows that with increasing air gap, there is increased impedance to heat flow in the build direction not only because of the increased fraction of air in the cross-section, but also because larger air gaps cause reduction in adherence between successive layers, and thus increased thermal contact resistance at the interfaces. Interestingly, once the air gap exceeds the raster width, the thermal contact resistance does not rise any further, and actually reduces somewhat. This is likely because once the air gap exceeds raster width, the nature of contact resistance between successive layers changes, since filaments in successive layers are no longer in direct contact with each other. Accurately accounting for this interesting, non-
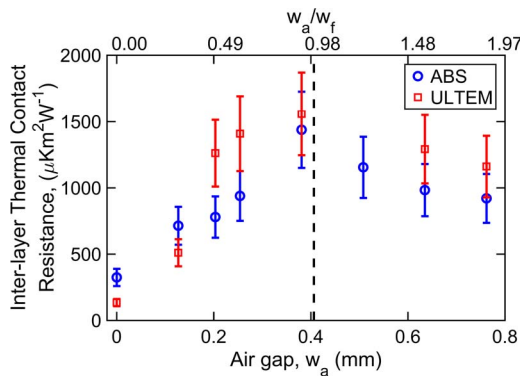
**Fig. 7.** Measured inter-layer thermal contact resistance as a function of air gap for both ABS and ULTEM filament materials. Dashed vertical line in this Figure shows the filament width, which is held constant at 0.41 mm. Top x-axis shows values of the ratio $w_a/w_f$.
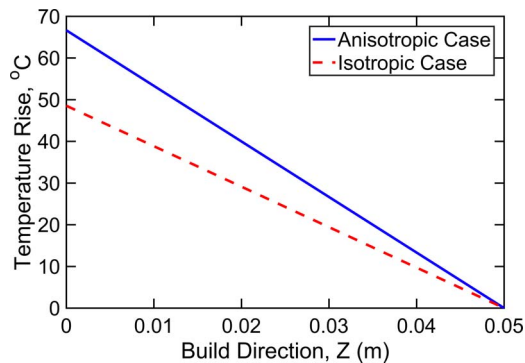


**Fig. 8.** Finite element simulations of the steady-state temperature field in an additively manufactured thin wall. Comparison between results based on isotropic and anisotropic thermal conductivity are shown.

monotonic effect of air gap on build-direction thermal contact resistance measured here is important for accurate thermal design. Careful consideration of these parameters may help design novel parts with ultra-low thermal conductivity without compromising on mechanical strength.

A set of finite element simulations are carried out in order to establish the importance of the measured anisotropy in thermal conduction in additively manufactured components reported here. A thin, additively manufactured insulating wall of thickness 50 mm is considered, wherein heat flux of 100 W/m$^2$ enters the wall on one face and flows across the wall, while the other face is maintained at constant temperature. It is assumed that the thickness of the wall is aligned with the build direction, $z$ axis as shown in Fig. 1. The wall is assumed to be large in the other two directions, as is the usual case for analyzing heat transfer through an infinite wall. Two simulations are carried out in order to demonstrate the importance of thermal conduction anisotropy. In the first case, the material is assumed to be isotropic, so that the values of $k_x$ and $k_z$ are the same. In the second case, the anisotropic nature of the material is accounted for, and the correct values of $k_x$ and $k_z$ based on measurements reported here are used. Fig. 8 plots the temperature field in the thin wall for both isotropic and anisotropic cases. The peak temperature in the first case, where $k_x$ and $k_z$ are incorrectly assumed to be equal to each other is much lower than the more realistic second case, where thermal anisotropy is accounted for. This shows that neglecting thermal anisotropy in the material that occurs due to the additive manufacturing process can lead to significant under-prediction of the temperature field in the material. As more and more functional parts begin to be additively manufactured, the effect of the manufacturing process on thermal properties, particularly on anisotropy in thermal conductivity must be correctly accounted for in order to ensure accurate design and operation of such parts.

## 5. Conclusions

While additive manufacturing is being investigated for building components for a wide variety of engineering applications, it is imperative to fully understand the effect of this unique manufacturing approach on thermal properties of the built part. This paper reports measurements of thermal conductivity of additively manufactured components, showing significant difference in the measured values in two orthogonal directions. Such anisotropy presents both challenges and opportunities, and regardless, must be accurately accounted for in design of additively manufactured components that must serve a thermal function. This paper shows that strong interfacial thermal contact resistance in the build direction is the fundamental reason for such anisotropy, and presents useful data on the dependence of this key parameter on process conditions. It is expected that theoretical insights on thermal conduction in additively manufactured parts from this work, as well as experimental data on anisotropic thermal conductivity and interfacial thermal contact resistance will facilitate the use of additive manufacturing processes for building components with unique thermal properties.

## Acknowledgments

## References

[1] D. Dimitrov, K. Schreve, N. de Beer, Advances in three dimensional printing –state of the art and future perspectives, Rapid Prototyp. J. 12 (2006) 136–147.

[2] D.T. Pham, R.S. Gault, A comparison of rapid prototyping technologies, Int. J. Mach. Tools Manuf. 38 (1998) 1257–1287.

[3] J.-P. Kruth, M.C. Leu, T. Nakagawa, Progress in additive manufacturing and rapid prototyping, CIRP Ann. Manuf. Technol. 2 (1998) 525–540.

[4] N. Guo, M.C. Leu, Additive manufacturing: technology, applications and research needs, Front. Mech. Eng. 8 (2013) 215–243.

[5] H. John, H. Martin, D. Brennan, D. Yahata, J.M. Hundley, J.A. Mayer, T.A. Schaedler, T.M. Pollock, 3D printing of high-strength aluminium alloys, Nature 549 (2017) 365–369.

[6] I. Zein, D.W. Hutmacher, K.C. Tan, S.H. Teoh, Fused deposition modeling of novel scaffold architectures for tissue engineering applications, Biomaterials 4 (2000) 1169–1185.

[7] S. Bose, S. Vahabzadeh, A. Bandyopadhyay, Bone tissue engineering using 3D printing, Mater. Today 12 (2013) 496–504.

[8] F.P.W. Melchels, J. Feijen, D.W. Grijpma, A review on stereolithography and its applications in biomedical engineering, Biomaterials 31 (2010) 6121–6130.

[9] D.W. Hutmacher, 'Scaffolds in tissue engineering bone and cartilage, Biomaterials 21 (2000) 2529–2543.

[10] K.V. Wong, A. Hernandez, A review of additive manufacturing, ISRN Mech. Eng. (2012) pp. 208760:1-10.

[11] B. Zhang, H. Liao, C. Coddet, Effects of processing parameters on properties of selective laser melting Mg–9% Al powder mixture, Mater. Des. 34 (2012) 753–758.

[12] N.K. Tolochko, M.K. Arshinov, A.V. Gusarov, V.I. Titov, T. Laoui, L. Froyen, Mechanisms of selective laser sintering and heat transfer in Ti powder, Rapid Prototyp. J. 9 (2003) 314–326.

[13] R. Anitha, S. Arunachalam, P. Radhakrishnan, Critical parameters influencing the quality of prototypes in fused deposition modelling, J. Mater. Process. Technol. 1–3 (2016) 385–388.

[14] B.N. Turner, R. Strong, S.A. Gold, A review of melt extrusion additive manufacturing processes: I. Process design and modeling, Rapid Prototyp. J. 3 (2014) 192–204.

[15] H. Kim, E. Park, S. Kim, B. Park, N. Kim, S. Lee, Experimental study on mechanical properties of single- and dual-material 3D printed products, Procedia Manuf. 10 (2017) 887–897.

[16] A.R. Torrado, D.A. Roberson, Failure analysis and anisotropy evaluation of 3D-printed tensile test specimens of different geometries and print raster patterns, J. Fail. Anal. Prev. 1 (2016) 154–164.

[17] C. Ziemian, M. Sharma, S. Ziemian, Anisotropic mechanical properties of ABS parts fabricated by fused deposition modelling, in: M. Gokcek (Ed.), Mechanical Engineering, InTech, 2012.

[18] A. Bellini, S. Guceri, Mechanical characterization of parts fabricated using fused deposition modeling, Rapid Prototyp. J. 4 (2003) 252–264.

[19] J.F. Rodríguez, J.P. Thomas, J.E. Renaud, Mechanical behavior of acrylonitrile butadiene styrene fused deposition materials modeling, Rapid Prototyp. J. 4 (2003) 219–230.

[20] S.H. Ahn, M. Montero, D. Odell, S. Roundy, P.K. Wright, Anisotropic material properties of fused deposition modeling of ABS, Rapid Prototyp. J. 8 (2002)

248–257.

[21] Z. Weng, J. Wang, T. Senthil, Lixin Wu, Mechanical and thermal properties of ABS/montmorillonite nanocomposites for fused deposition modeling 3D printing, Mater. Des. 102 (2016) 276–283.

[22] K.-P. Weiss, N. Bagrets, C. Lange, W. Goldacker, J. Wohlgemuth, Thermal and mechanical properties of selected 3D printed thermoplastics in the cryogenic temperature regime, IOP Conf. Ser. Mater. Sci. Eng. 102 (2015) 012022.

[23] C. Shemelya, A. De La Rosa, A. Torrado, K. Yu, J. Domanowski, P. Bonacuse, R. Martin, M. Juhasz, F. Hurwitz, R. Wicker, B. Conner, E. MacDonald, D.A. Roberson, Anisotropy of thermal conductivity in 3D printed polymer matrix

composites for space based cube satellites, Addit. Manuf. 16 (2017) 186–196.

[24] S.-Y. Chung, D. Stephan, M.A. Elrahman, T.-S. Han, Effects of anisotropic voids on thermal properties of insulating media investigated using 3D printed samples, Constr. Build. Mater. 111 (2016) 529–542.

[25] V. Vishwakarma, C. Waghela, Z. Wei, R. Prasher, S.C. Nagpure, J. Li, F. Liu, C. Daniel, A. Jain, Heat transfer enhancement in a Lithium-ion cell through improved material-level thermal transport, J. Power Sources 300 (2015) 123–131.

[26] A.S. El-Gizawy, S. Corl, B. Graybill, Process-induced properties of FDM products, Proceedings of The ICMET, International Conference on Mechanical Engineering and Technology Congress & Exposition, Paris, France, 2011.